Erciyes Üniversitesi
Fen Bilimleri Enstitüsü Dergisi
Cilt 38, Sayı 3, 2022

Erciyes University
Journal of Institue Of Science and
Technology Volume 38, Issue 3, 2022

iSeg-WNet: Volumetric Segmentation of Infant Brain MRI Images

Gaffari Çelik[*1]

[*1] Agri Ibrahim Cecen University Vocational School Department of Computer Technology, AĞRI

(Alınış / Received: 06.04.2022, Kabul / Accepted: 25.08.2022, Online Yayınlanma / Published Online: 30.12.2022)

Keywords
Deep Learning,
CNN,
Segmentation,
Dice Loss,
3D MRI Segmentation,
iseg-2019,
iseg-2017

Abstract: Examination of infant brain development is extremely important in terms of early diagnosis of possible brain dysfunctions. Brain MRI structures are usually studied by segmentation into white matter (WM), gray matter (GM) and cerebrospinal fluid (CSF) tissues. Low-density contrast between tissues in infant brains complicates the segmentation process. It is seen that the segmentation process is done very well with the Deep Learning architectures that have been developed recently. In this study, an architecture called Deep Learning-based iSeg-WNet is proposed for segmentation of infant brain MRI images. Appropriate hyperparameters were determined by different studies and the performances of different architectures were compared. Performance comparison was made according to Dice metric. In experimental studies, it has been observed that the use of MRI images in T1w and T2w images together increases the segmentation performance. At the same time, high performance was obtained by using Dice Loss as a cost function and MinMax normalization as a data normalization process. When the segmentation performances of different architectures are examined, it is seen that the proposed architecture segments CSF (%91.8), GM (%89) and WM (%86) tissues with the highest success. The proposed architecture is available at https://github.com/GaffariCelik/iSeg-WNet.

iSeg-WNet: Bebek Beyin MRI Görüntülerinin Volumetrik Bölütlemesi

Anahtar Kelimeler
Derin Öğrenme,
CNN,
Bölütleme,
Dice Loss,
3D MRI Bölütleme,
iseg-2019,
iseg-2017

Öz: Bebek beyin gelişiminin incelenmesi, doğabilecek beyin fonksiyon bozuklarının erken teşhisi açısından son derece önemlidir. Beyin MRI yapıları genellikle beyaz madde (WM), gri madde (GM) ve beyin omurilik sıvısı (CSF) dokularına bölütlenmesi ile işlemi ile incelenmektedir. Bebek beyinlerinde dokular arasındaki düşük yoğunluklu kontrast bölütleme işlemini zorlaştırmaktadır. Son dönemlerde geliştirilen Derin Öğrenme mimarileri ile bölütleme işleminin son derece çok iyi yapıldığı görülmektedir. Bu çalışmada bebek beyin MRI görüntülerinin bölütlenmesi için Derin Öğrenme tabanlı iSeg-WNet adıyla bir mimari önerilmiştir. Farklı çalışmalar ile uygun hiperparametreler belirlenmiş ve farklı mimarilerin performansları karşılaştırılmıştır. Performans karşılaştırılması Dice metriğine göre yapılmıştır. Yapılan deneysel çalışmalarda, T1w ve T2w çekimlerdeki MRI görüntülerinin beraber kullanılması bölütleme performansının artırdığı gözlemlenmiştir. Aynı zamanda maliyet fonksiyonu olarak Dice Loss ve veri normalizasyon işlemi olarak da MinMax normalizasyonun kullanılması ile yüksek başarım elde edilmiştir. Farklı mimarilerin bölütleme performansları incelendiğinde, önerilen mimari ile CSF(%91.8), GM (%89) ve WM (%86) dokularını en yüksek başarı ile bölütlediği görülmüştür. Önerilen mimariye https://github.com/GaffariCelik/iSeg-WNet adresinden erişilebilir.

*Corresponding Author, email: gcelik2014@gmail.com

1. Introduction

The advancement of brain imaging techniques has played an important role in the study of brain anatomy and functions. Magnetic Resonance Imaging (MRI) technique is widely used to characterize disorders in brain structure and to extract structural information from various contrast images. Brain MRI segmentation plays an important role in analyzing changes in brain structures that occur over time. Brain MRI segmentation is very important in the pre-diagnosis of Alzheimer's, Parkinson's, Schizophrenia Multiple Sclerosis and other brain diseases, and the detection of diseased tissues in the post-diagnostic stages [1]. However, brain MRI segmentation is a difficult task due to the presence of noise, density irregularity, movement, and partial volume effects during image acquisition [2].

Thanks to the advances in MRI imaging of the infant brain anatomy, it was ensured that a healthy image was obtained with the obtained high-resolution images. MRI images can be viewed in different scans such as T1-weighted (T1w), T2-weighted (T2w), resting state functional MRI (rsfMRI), and diffusion-weighted MRI (dMRI). MRI images taken in different modalities offer important opportunities in the study of brain anatomy and analysis of early postnatal brain development. There are significant differences in MRI images according to age groups. This difference is clearly understood in Figure 1. Baby brain images are more difficult to process and analyze than adult brains. There are great differences in a baby's brain structure, brain size, density changes, intra-tissue inhomogeneity, tissue contrast and regionally different tissue images depending on age [3-6]. However, in infants' brain MRIs, increased noise, low contrast between tissues, and continued white matter myelination lead to misclassification of brain tissues [7].

In examining both normal and abnormal early brain development of infants, it is important to examine brain MRIs by segmenting white matter (WM), gray matter (GM) and cerebrospinal fluid (CSF) tissues [8]. Early examination of brain growth patterns and morphological changes in neurologically developmental disorders, accurate segmentation of MRI images into WM, GM and CSF tissues is crucial [9]. With segmentation, it is aimed to segment brain tissues. This process is performed manually by clinical experts. However, this process, which is an extremely sensitive issue, is time consuming, subject to intra- or inter-observational variables and requires specialist physicians. Consistent results have been obtained with automatic segmentation methods developed using deep learning methods recently. This is considered as alternative methods for manual partitioning problems [7,10].

Deep learning has a deep network architecture consisting of many layers, unlike neural networks that can have a single layer. Having such a deep network architecture enables a detailed feature map to be extracted from the input data by self-learning, as opposed to manual feature extraction from input data in machine learning algorithms. Deep learning performs impressively on large amounts of data. In addition, this success has been greatly contributed by the rapid development of graphics processing units (GPUs). Due to rapid advances in the computing power of GPUs, it has enabled the rapid development of complex deep learning models [6]. Deep learning, image resolution [11], brain MRI segmentation [10, 12, 13], image registration [14], generating images from EEG signal [15], mammographic lesions detection [16], lung segmentation [17, 18], classification of white blood cells [19], brain disease classification [20], detection of arrhythmia [21-23] and detecting pneumonia from chest X-ray images [24], determination of basic physical movements of people [25], Classification of Breast Cancer [26] and breast lymph node segmentation [27].

Our main contributions in this study can be summarized as follows:

- Development of a new deep learning-based architecture that segments 3D Brain MRIs
- Segmentation of pediatric brain MRIs using different datasets
- Segmentation of MRI images in different modalities (T1w,T2w) and examination of their success
- Performance evaluation of the proposed architecture in different Hyperparameters
- Evaluation of 3D MRI segmentation performances of different architectures

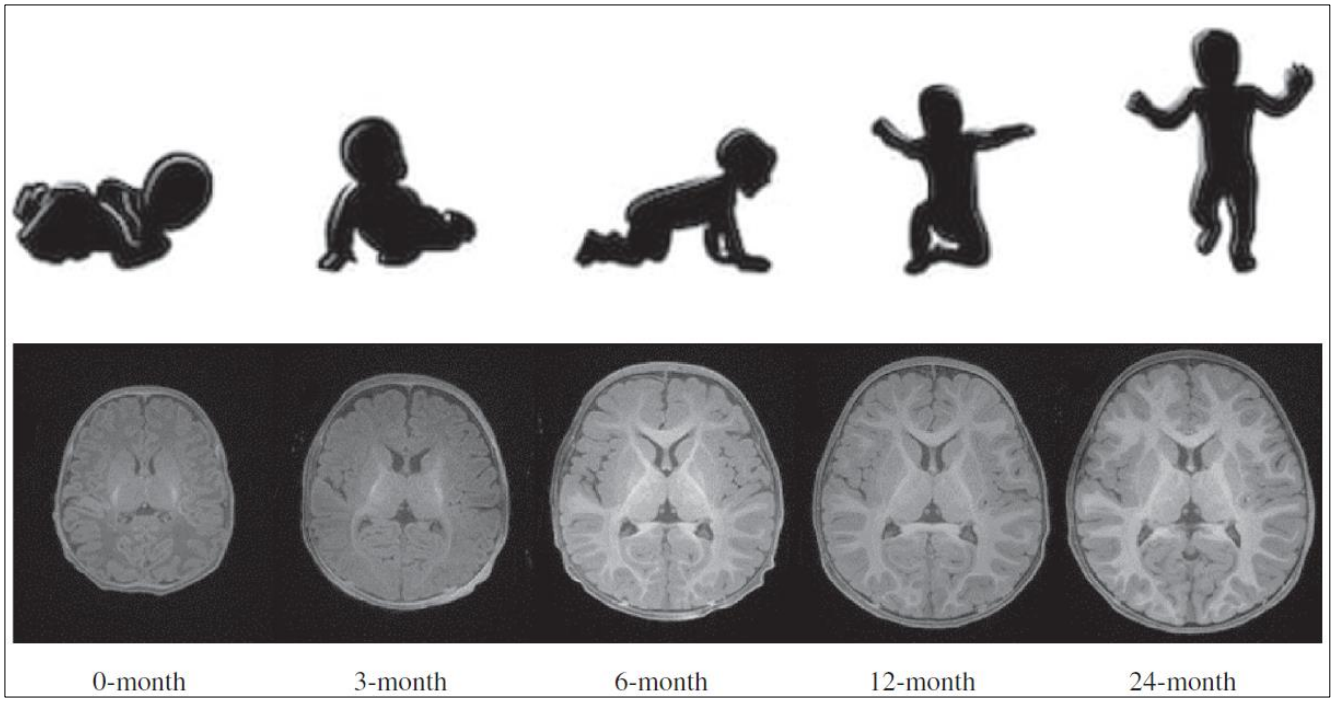

Figure 1. Baby brain MRI sample images taken between 0-24 months at T1w weight [6].

2. Material and Method

In this study, two datasets, iseg-2017 [9] and iseg-2019 [28], were used for segmentation of child brain MRI images. A CNN-based architecture is proposed for segmentation of MRI images.

2.1. Material

iseg-2017 [9] and iseg-2019 [28] datasets were published by the MICCAI (Medical Image Computing and Computer-Aided Intervention) community to conduct research on brain tissue segmentation, which includes MRI images of the 6-month-old infant brain. The characteristics of the datasets are presented in Table 1. The datasets consist of 10 MRIs taken in the T1w and T2w modalities. Each data sample has dimensions of 144 × 192 × 256 and a resolution of 1.0 ×1.0 ×1.0 mm3. In addition, each MRI is supplied with masks (groundTrue, GT) labeled to three brain tissues, GM, WM, and CSF, to guide the learning of algorithms during the training phase. In the iseg-2017 dataset, the background (BGR) is labeled 0, the CSF region 10, the GM region 150, and the WM region 250. In the iseg-2019 dataset, it is labeled as BGR 0, CSF region 1, GM region 2, and WM region 3.

Table 1. Properties of data sets

Data Sets	MRI dimension	Voxel size (mm3)	Modalities	Number of MRI	Labelling
iseg-2017	144x192x256	1.0x1.0x1.0	T1w, T2w	10	BGR:0, CSF:10, GM:150, WM:250
iseg-2019	144x192x256	1.0x1.0x1.0	T1w, T2w	10	BGR:0, CSF:1, GM:2, WM:3

Table 1. shows that the labeling of brain regions (GT) of the data sets is different. GTs are relabeled according to Eq. 1.

$$GT^{new}_{iseg-2017}(x) = \begin{cases} 1 & if\ GT_{iseg-2017}(x) == 10 \\ 2 & else\ if\ GT_{iseg-2017}(x) == 150 \\ 3 & else\ if\ GT_{iseg-2017}(x) == 250 \\ 0 & else \end{cases} \quad (1)$$

Figure 2 shows the modalities of an image taken from an exemplary MRI and the segmented GT. In GT, red indicates CSF tissue, blue indicates WM tissue, and green indicates GM tissue. Datasets are available at https://iseg2017.web.unc.edu/ and https://iseg2019.web.unc.edu/.

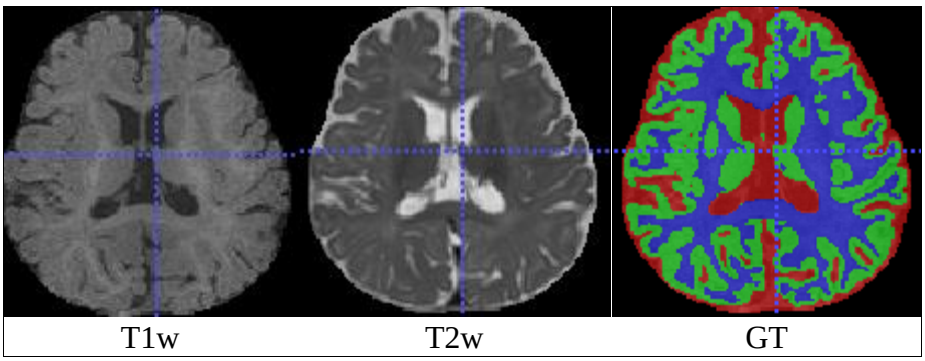

Figure 2. T1w, T2w modalities and mask(GT) of an MRI image. Red indicates CSF tissue, blue indicates WM tissue, and green GM tissue.

2.2 Method

Although Machine learning has shown high success in various fields, its performance is largely dependent on the features extracted from the training datasets, which is seen as a significant disadvantage. It has received a lot of attention recently that deep learning architectures automatically extract the best features from the raw input data with the help of convolutional neural network (CNN) without any preprocessing. CNNs form the basic building block of Deep learning algorithms [29, 30]. CNNs architectures are considered feedforward networks consisting of convolution layers, pool layers, and fully connected layers, as shown in Figure 3. These networks provide information flow from the input layer to the output layer. While the convolution and pooling layers feature mapping from the input data, the last fully connected layer is fed in a coordinated manner by the previous fully connected layers, giving the information of each class [31].

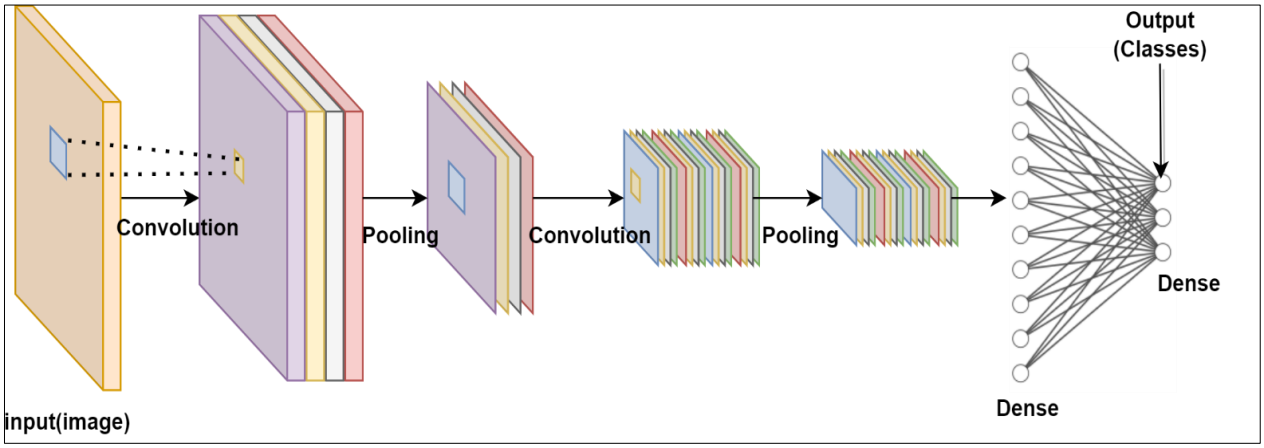

Figure 3. Basic lines of CNN architecture

In this study, a CNN-based architecture is proposed that enables segmentation of infant brain MRI images. This architecture, called iSeg-WNet, is shown in Figure 4. The architecture consists of input, encoder, bottleneck, decoder and output stages. In the entry phase, MRIs in T1w and T2w modalities are given as input. After the input data is passed through the encoder, bottleneck and decoder processes, respectively, the same processes are repeated and given to the output unit.

In the encoder part, convolution, normalization, activation and refutation processes were applied gradually. Except for the last stage, decay was used after the activation process in all the other stages. In the first and second stages, the 3D Convolution process with stride 2 and kernel size 3 was used. After the convolution process, instance normalization [32], Leaky ReLU activation function and dropout with a ratio of 0.2 were used, respectively. At each stage, provided that the previous operations and parameters are kept constant, only the stride value is renewed in the 3D convolution process by giving 1 to it. In the last stage, the kernel ratio value of 5 is given in the 3D convolution process. The other processes were repeated and connected to the Bottlenek section. In the encoder section, the initial filter number was given 64 and increased 2 times at each stage. The feature map was expanded with the progressively increasing number of filters. In addition, with the stride parameter, the data size is reduced and unnecessary features are eliminated.

In the bottleneck section that combines the encoder and decoder, the number of filters is 256 and the kernel size is 5, and 3D convolution process is applied. After the convolution process, the result obtained by applying the

normalization and activation process is combined with the result of the initial convolution process. The same operations were repeated four times and connected to the decoder section.

With the Conv3DTranspose operation in the decoder section, both the convolution operation and the data size are gradually enlarged. After the Conv3DTranspose process, the results obtained by applying normalization and activation processes are combined with the result at the same stage in the Encoder section. In this way, it is ensured that the features are reused. After the assembly stage, the dropout process was carried out. At the same stage, provided that the number of filters remains the same, 3D convolution, normalization, activation and decay processes are applied. These processes were repeated by gradually reducing the number of filters by two times. Encoder, bottleneck and decoder sections were repeated for the second time and connected to the output section. After the Conv3DTranspose process in the output section, the segmentation of the brain tissue sections was performed with the softmax activation function. Dice Loss cost function was used for the training of the architecture [33].

$$L_{Dice} = \frac{2|X \cap Y|}{|X| + |Y|} \tag{2}$$

Here, X and Y represent GT and segmentation result information.

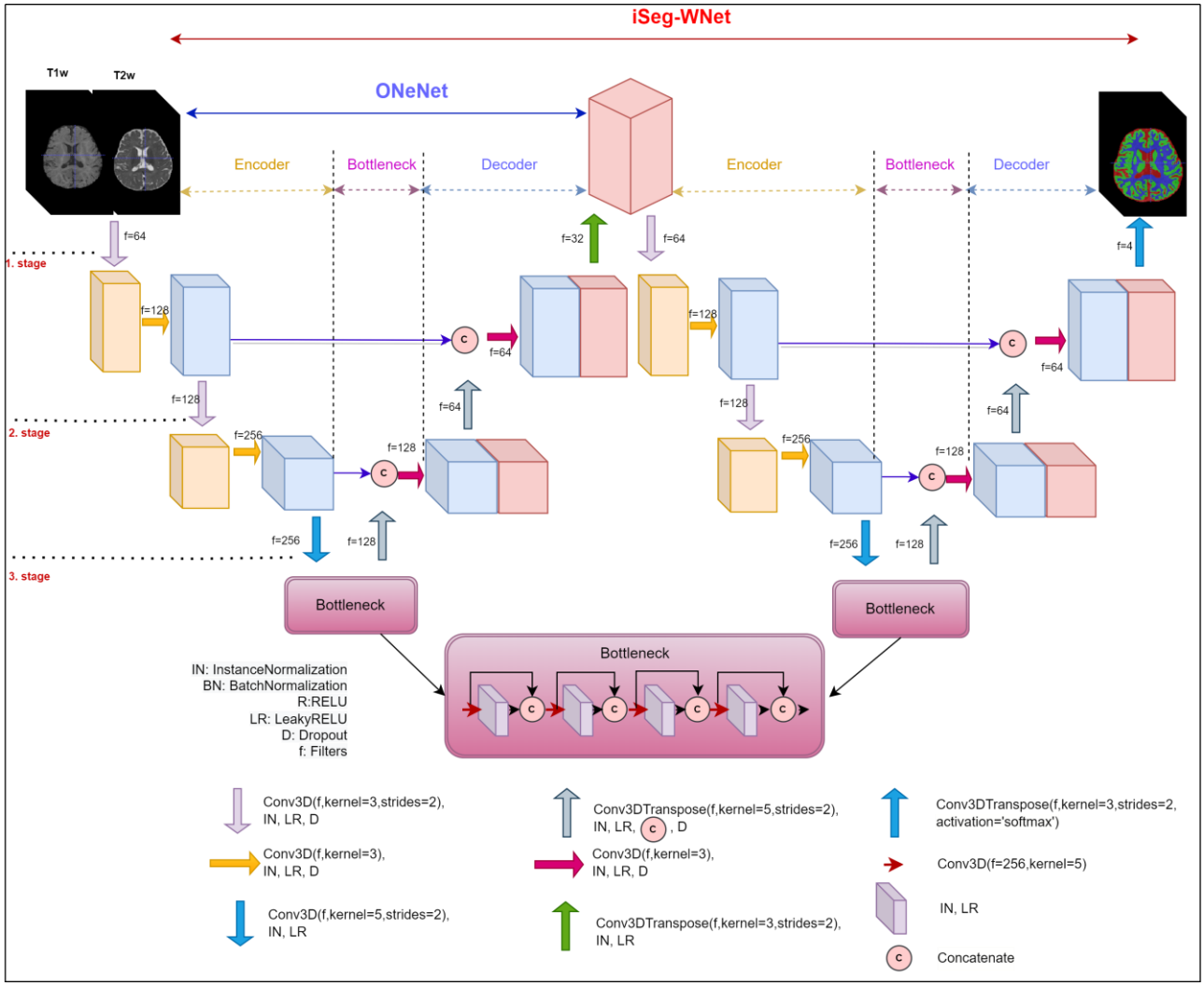

Figure 4. iSeg-WNet architecture

OneNet architecture has an architecture similar to UNet architecture. The OneNet architecture is the first part of the iSeg-WNet architecture, as shown in Figure 4. Only in the last layer, the number of filters is 4 and the softmax optimization function is used. Softmax activation function is expressed mathematically as in Eq. 3 [34]:

$$Z^k = \frac{e^{x^k}}{\sum_{i=1}^{n} e^{x^n}} \tag{3}$$

Here, x and n represent the input vector and the number of classes, respectively. Up to k=1 … . n and Z represents the output vector. The sum of the values of Z is 1.

3. Results

In this section, different studies have been carried out using the iSeg-WNet architecture for segmentation of child brain MRIs. First of all, a study was conducted according to the different modalities in the datasets. The goal here is to find the appropriate modality for appropriate tissue segmentation. In the second study, a study was carried out according to the loss functions in order to increase the segmentation performance. Thirdly, performance evaluation was made according to different normalization processes. Finally, after the appropriate parameters were determined, the successes of different architectures were evaluated.

The most widely used Dice metric in the literature was used to evaluate the performances of the studies. The Dice metric is given in Equation 2. In the studies, 80% of the data set is reserved for training and 20% for testing. An out-of-memory error occurs when training architectures without any changes in MRI dimensions during the training phase. To solve this problem, MRIs are cropped in 128x144x128 size and given as an input to architectures, provided that they remain within the brain region. The Adam (Learning_rate=0.0001) optimization function is used as the optimization function in the architectures. In each work, Architectures 180 min. has been trained. Weights were recorded every 60 minutes and their performance was observed.

In the first application, it was made on how MRIs taken in different modalities affect segmentation performance. As an introduction to the iSeg-WNet architecture, T1w, then T2w, and finally both modalities were given to the architecture network together and trained separately. In this application, categorical crossentropy is used as a cost function. The results of the first application to select the best modality as data input are given in Table 2. When the results are examined, it is seen that the highest performance is achieved when T1w and T2w modalities are given together as an introduction to architecture. We can say that a high performance has been achieved with the T1w weight. A lower performance was obtained with the T2w modality. Categorical crossentropy can be expressed as [35]:

$$L_{CE} = \sum_{i=1}^{C} y_{true}\, log(y_{pre}) \tag{4}$$

Here $y_{pred} \in (0, 1)$, i. for example the forecast distribution and $y_{true} \in (0, 1)$, i. represents the true distribution of the sample.

Table 2. Performance evaluation according to modalities in different modalities using the categorical crossentropy cost function

		T1w				T2w				T1w+T2w			
Train(min.)	Mri	CSF	GM	WM	Avg	CSF	GM	WM	Avg	CSF	GM	WM	Mean
60	1	0,894	0,868	0,854	0,872	0,89	0,824	0,752	0,822	0,889	0,876	0,868	0,878
	2	0,894	0,868	0,854	0,872	0,83	0,79	0,776	0,799	0,914	0,879	0,825	0,873
	3	0,911	0,87	0,813	0,865	0,89	0,824	0,752	0,822	0,914	0,879	0,825	0,873
	4	0,912	0,87	0,813	0,865	0,83	0,79	0,776	0,799	0,889	0,876	0,868	0,878
	Mean	0,903	0,869	0,834	0,87	0,86	0,807	0,764	0,81	0,902	0,878	0,847	**0,876**
120	1	0,909	0,877	0,867	0,884	0,895	0,883	0,763	0,847	0,926	0,883	0,83	0,88
	2	0,923	0,874	0,816	0,871	0,938	0,796	0,786	0,84	0,926	0,883	0,83	0,88
	3	0,909	0,877	0,867	0,884	0,895	0,833	0,763	0,83	0,895	0,877	0,875	0,882
	4	0,923	0,874	0,816	0,871	0,838	0,796	0,786	0,807	0,895	0,877	0,875	0,882
	Mean	0,916	0,876	0,842	0,878	0,892	0,827	0,775	0,831	0,911	0,88	0,853	**0,881**
180	1	0,923	0,879	0,82	0,874	0,851	0,806	0,79	0,816	0,907	0,885	0,879	0,89
	2	0,923	0,879	0,82	0,874	0,899	0,84	0,766	0,835	0,931	0,886	0,833	0,883
	3	0,916	0,884	0,869	0,89	0,899	0,84	0,766	0,835	0,931	0,886	0,833	0,883
	4	0,916	0,884	0,869	0,89	0,851	0,806	0,79	0,816	0,907	0,885	0,879	0,89
	Mean	0,92	0,882	0,845	0,882	0,875	0,823	0,778	0,825	0,919	0,886	0,856	**0,887**

After determining the data in the appropriate modality in the first application, T1w and T2w modalities are given together as data input for the training of architectures and testing in other studies.

In the second application, the performance of the iSeg-WNet architecture was examined according to different cost functions and the results are presented in Table 3. Although the results are close to each other, it is seen that the highest performance is obtained with Dice Loss as a cost function.

Table 3. Performance evaluation according to loss functions

		Categorical_Loss				Dice_Loss_class_weight [33]				Dice_Loss			
Train(min.)	Mri	CSF	GM	WM	Mean	CSF	GM	WM	Mean	CSF	GM	WM	Mean
60	1	0,889	0,876	0,868	0,878	0,882	0,865	0,86	0,869	0,897	0,872	0,868	0,879
	2	0,914	0,879	0,825	0,873	0,904	0,866	0,816	0,862	0,915	0,874	0,823	0,871
	3	0,914	0,879	0,825	0,873	0,904	0,866	0,816	0,862	0,915	0,874	0,823	0,871
	4	0,889	0,876	0,868	0,878	0,882	0,865	0,86	0,869	0,89	0,872	0,868	0,877
	Mean	0,902	0,878	0,847	**0,876**	0,893	0,866	0,838	0,866	0,904	0,873	0,846	0,874
120	1	0,926	0,883	0,83	0,88	0,889	0,875	0,872	0,879	0,897	0,883	0,878	0,886
	2	0,926	0,883	0,83	0,88	0,889	0,875	0,872	0,879	0,897	0,883	0,878	0,886
	3	0,895	0,877	0,875	0,882	0,918	0,878	0,827	0,874	0,926	0,885	0,831	0,881
	4	0,895	0,877	0,875	0,882	0,918	0,878	0,827	0,874	0,926	0,885	0,831	0,881
	Mean	0,911	0,88	0,853	0,881	0,904	0,877	0,85	0,877	0,912	0,884	0,855	**0,884**
180	1	0,907	0,885	0,879	0,89	0,893	0,881	0,878	0,884	0,906	0,887	0,88	0,891
	2	0,931	0,886	0,833	0,883	0,919	0,883	0,831	0,878	0,906	0,887	0,88	0,891
	3	0,931	0,886	0,833	0,883	0,919	0,883	0,831	0,878	0,931	0,889	0,835	0,885
	4	0,907	0,885	0,879	0,89	0,893	0,881	0,878	0,884	0,931	0,889	0,835	0,885
	Mean	0,919	0,886	0,856	0,887	0,906	0,882	0,855	0,881	0,919	0,888	0,858	**0,888**

In the third application, performance evaluation was made according to the normalization processes in the data preprocessing stage. The proposed architecture is trained with different normalization processes and the results are given in Table 4. When the results are examined, it is seen that the highest MinMax normalization is achieved with a performance of 88.9%. Minmax normalization is given in Eq. 5, z-score normalization is given in Eq. 6 [36].

$$v' = \frac{v - min_A}{man_A \; - \; min_A} \tag{5}$$

$$z = \frac{v - \mu_A}{\sigma_A} \tag{6}$$

Here, v' and z represent the normalized feature, and v represents the original feature. Expression A properties, min_A is the smallest value of property A, max_A is the largest value of property A; $\mu_A$indicates the mean and σ_A the standard deviation.

Table 4. Segmentation results according to different normalization processes in the data preprocessing stage

		Notnormalization				MinMaxNorm.				Zscore_Norm.			
Train(min.)	Mri	CSF	GM	WM	Mean	CSF	GM	WM	Mean	CSF	GM	WM	Mean
60	1	0,897	0,872	0,868	0,879	0,891	0,877	0,868	0,879	0,902	0,873	0,822	0,866
	2	0,915	0,874	0,823	0,871	0,891	0,877	0,868	0,879	0,89	0,882	0,875	0,882
	3	0,915	0,874	0,823	0,871	0,916	0,881	0,83	0,876	0,902	0,873	0,822	0,866
	4	0,89	0,872	0,868	0,877	0,916	0,881	0,83	0,876	0,89	0,882	0,875	0,882
	Mean	0,904	0,873	0,846	0,874	0,904	0,879	0,849	**0,877**	0,896	0,878	0,849	0,874
120	1	0,897	0,883	0,878	0,886	0,901	0,884	0,878	0,888	0,902	0,89	0,882	0,891
	2	0,897	0,883	0,878	0,886	0,901	0,884	0,878	0,888	0,917	0,883	0,829	0,876
	3	0,926	0,885	0,831	0,881	0,927	0,888	0,836	0,884	0,917	0,883	0,829	0,876
	4	0,926	0,885	0,831	0,881	0,927	0,888	0,836	0,884	0,902	0,89	0,882	0,891
	Mean	0,912	0,884	0,855	0,884	0,914	0,886	0,857	**0,886**	0,91	0,887	0,856	0,884
180	1	0,906	0,887	0,88	0,891	0,931	0,892	0,839	0,887	0,912	0,882	0,829	0,874
	2	0,906	0,887	0,88	0,891	0,904	0,888	0,881	0,891	0,912	0,882	0,829	0,874
	3	0,931	0,889	0,835	0,885	0,931	0,892	0,839	0,887	0,899	0,891	0,883	0,891
	4	0,931	0,889	0,835	0,885	0,904	0,888	0,881	0,891	0,899	0,891	0,883	0,891
	Mean	0,919	0,888	0,858	0,888	0,918	0,89	0,86	**0,889**	0,906	0,887	0,856	0,883

After obtaining the best hyperparameters that increase the success of the iSeg-WNet architecture, a new application has been carried out to compare the performances of different architectures. In this application, the performances of iSeg-WNet, OneNet and 3D-UNet [37] architectures were compared by keeping the hyperparameters the same, and the results are shown in Table 5. U-Net architecture consists of encoder,

bottleneck and decoder parts. The encoder section consists of 3 stages, and at each stage, convolution, RELU activation and subsampling (maxpooling) processes are applied. The bottleneck section acts as a transition that connects the Encoder and Decoder sections to each other. This is the section where the relu activation operations are applied after the convolution and each convolution operation. Another part, Decoder, has a 3-stage structure. At each stage, the oversampling, convolution and relu operation is applied after each convolution operation. At the same time, the feature outputs of the encoder section at each stage are transferred to the decoder section and reused.

When the results in Table 5 are examined, it is seen that the proposed architecture has a higher success rate of 88.9% compared to other architectures.

Table 5. Segmentation results of different architectures

		3D U-Net [37]				OneNET				Our(iSeg-WNet)			
Train(min.)	Mri	CSF	GM	WM	Mean	CSF	GM	WM	Mean	CSF	GM	WM	Mean
60	1	0,922	0,883	0,776	0,86	0,88	0,868	0,864	0,871	0,891	0,877	0,868	0,879
	2	0,897	0,862	0,826	0,862	0,908	0,874	0,822	0,868	0,891	0,877	0,868	0,879
	3	0,922	0,883	0,776	0,86	0,88	0,868	0,864	0,871	0,916	0,881	0,83	0,876
	4	0,922	0,883	0,776	0,86	0,908	0,874	0,822	0,868	0,916	0,881	0,83	0,876
	Mean	0,916	0,878	0,789	0,861	0,894	0,871	0,843	0,869	0,904	0,879	0,849	**0,877**
120	1	0,924	0,884	0,786	0,865	0,924	0,877	0,819	0,873	0,901	0,884	0,878	0,888
	2	0,894	0,86	0,832	0,862	0,898	0,869	0,858	0,875	0,901	0,884	0,878	0,888
	3	0,894	0,86	0,832	0,862	0,924	0,877	0,819	0,873	0,927	0,888	0,836	0,884
	4	0,924	0,884	0,786	0,865	0,898	0,869	0,858	0,875	0,927	0,888	0,836	0,884
	Mean	0,909	0,872	0,809	0,863	0,911	0,873	0,839	0,874	0,914	0,886	0,857	**0,886**
180	1	0,923	0,884	0,793	0,867	0,917	0,87	0,808	0,865	0,931	0,892	0,839	0,887
	2	0,923	0,884	0,793	0,867	0,897	0,86	0,844	0,867	0,904	0,888	0,881	0,891
	3	0,894	0,861	0,836	0,864	0,897	0,86	0,844	0,867	0,931	0,892	0,839	0,887
	4	0,894	0,861	0,836	0,864	0,917	0,87	0,808	0,865	0,904	0,888	0,881	0,891
	Mean	0,909	0,873	0,815	0,866	0,907	0,865	0,826	0,866	**0,918**	**0,89**	**0,86**	**0,889**

Example images obtained as a result of segmentation of an MRI by the architectures are given in Figure 5. The first line shows the whole brain, the second, third and fourth lines show the axial, coronal and sagittal images, respectively.

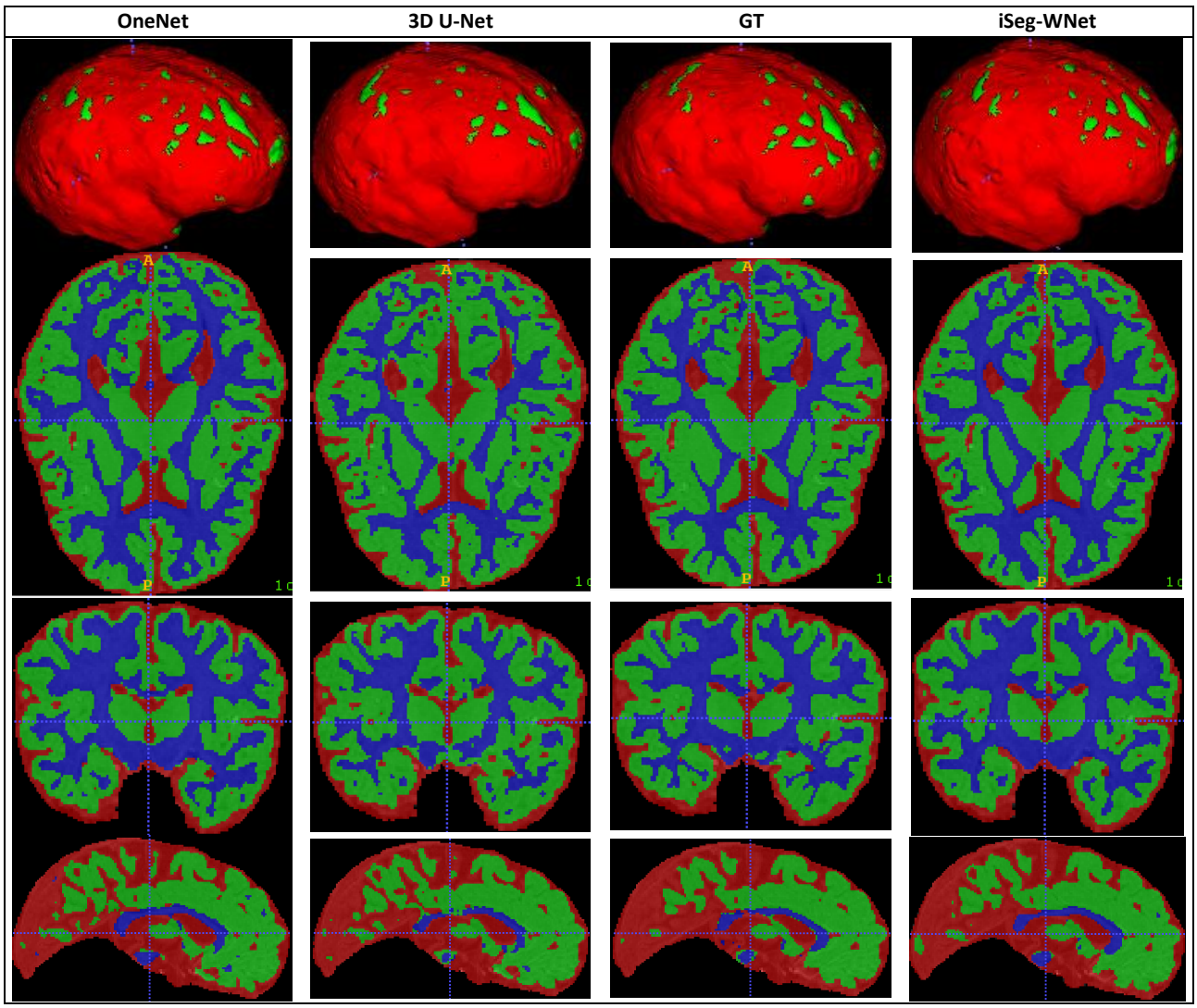

Figure 5. Sample images obtained as a result of segmentation of a sample MRI from the test dataset by architectures

4. Discussion and Conclusion

In the study of the development of infant brains, prevention of brain growth patterns and morphological changes in neurological developmental disorders is very important. In this respect, it is important to examine and correctly segment the brain tissues of the white matter (WM), gray matter (GM) and cerebrospinal fluid (CSF) brain regions. In this study, a deep learning-based architecture called iSeg-WNet is proposed, which provides segmentation of brain tissues using the iseg-2017 and iseg-2019 datasets containing 6-month 3D brain MRI images. The iseg-WNet architecture is formed by repeating these structures based on Encoder, Bottlenech and Decoder structures twice.

Different experimental studies have been carried out with the proposed architecture and appropriate hyperparameters have been found. In addition, the appropriate modality that will increase the segmentation performance has been determined for MRI images with different modalities (T1w, T2w) in the datasets. Finally, the performances of different architectures are compared.

With the first experimental study, the appropriate modality was determined. Accordingly, when the images in T1w and T2w modalities were given together as an input to the architecture, it was seen that it showed the highest success with an average success rate of 88.7%. In the second application, the performance evaluation of the proposed architecture was made according to different cost functions. The highest success rate of 88.8% was achieved with the Dice_Loss cost function. In the third application made according to different normalization processes, the highest performance was obtained by using MinMax normalization with a success rate of 88.9%.
In the last experimental study to examine the performances of different architectures, it was seen that the iSeg-WNet architecture exhibited the highest segmentation performance with 91.8% CSF tissue, 89% GM tissue, 86% WM tissue and 88.9% on average.

References

[1] Ghosal ,P. Chowdhury, Kumar, T. A. Bhadra, A. K. Chakraborty, J. Nandi, D. 2021. MhURI:A Supervised Segmentation Approach to Leverage Salient Brain Tissues in Magnetic Resonance Images. Comput. Methods Programs Biomed., 200, 105841, doi: 10.1016/j.cmpb.2020.105841.

[2] Balafar, M. A. Ramli,A. R. Saripan, M. I. Mashohor, S. 2010. Review of brain MRI image segmentation methods. Artif. Intell. Rev., 33(3), 261–274, 2010, doi: 10.1007/s10462-010-9155-0.

[3] Jenkinson, M. Beckmann, C. F. Behrens, T. E. J. Woolrich, M. W. Smith, S. M. 2012. FSL, NeuroImage, 62, 782–790, doi: 10.1016/j.neuroimage.2011.09.015.

[4] Dai,Y. Shi, F. Wang,L. Wu, G. Shen, D. 2013. IBEAT: A toolbox for infant brain magnetic resonance image processing. Neuroinformatics, 11(2), 211–225, doi: 10.1007/s12021-012-9164-z.

[5] Fischl, B. 2012. FreeSurfer. Neuroimage, 62(2), 774–781, doi: 10.1016/j.neuroimage.2012.01.021.

[6] Mostapha, M. Styner, M. 2019. Role of deep learning in infant brain MRI analysis. Magn. Reson. Imaging, 64(June), 171–189, doi: 10.1016/j.mri.2019.06.009.

[7] Wang, L. et al. 2014. Segmentation of neonatal brain MR images using patch-driven level sets. Neuroimage, 84, 141–158, doi: 10.1016/j.neuroimage.2013.08.008.

[8] Dolz, J. Desrosiers, C. Wang, L. Yuan, J. Shen, D. Ayed, I. B. 2020. Deep CNN ensembles and suggestive annotations for infant brain MRI segmentation. Comput. Med. Imaging Graph., 79, 101660, doi: 10.1016/j.compmedimag.2019.101660.

[9] Wang, L. et al. 2019. "Benchmark on automatic six-month-old infant brain segmentation algorithms: The iSeg-2017 challenge. IEEE Trans. Med. Imaging, 38(9), 2219–2230, doi: 10.1109/TMI.2019.2901712.

[10] Bui, T. D. Shin, J. Moon, T. 2019. Skip-connected 3D DenseNet for volumetric infant brain MRI segmentation. Biomed. Signal Process. Control, 54, 101613, 2019, doi: 10.1016/j.bspc.2019.101613.

[11] Çelik, G. Talu, M. F. 2020. Resizing and cleaning of histopathological images using generative adversarial networks. Phys. A Stat. Mech. its Appl., 554, 122652, doi: 10.1016/j.physa.2019.122652.

[12] Çelik, G. Talu, M. F. 2022. A new 3D MRI segmentation method based on Generative Adversarial Network and Atrous Convolution. Biomed. Signal Process. Control, 71(PA), 103155, doi: 10.1016/j.bspc.2021.103155.

[13] Akkus, Z. Galimzianova, A. Hoogi, A. Rubin, D. L. Erickson, B. J. 2017. Deep Learning for Brain MRI Segmentation: State of the Art and Future Directions. J. Digit. Imaging, 30(4), 449–459, doi: 10.1007/s10278-017-9983-4.

[14] Yang, X. Kwitt, R. Styner, M. Niethammer, M. 2017. Quicksilver: Fast predictive image registration – A deep learning approach. Neuroimage, 158(July), 378–396, doi: 10.1016/j.neuroimage.2017.07.008.

[15] Çelik, G. Talu, M. F. 2021. Generating the image viewed from EEG signals. Pamukkale Univ. J. Eng. Sci., 27(2), 129–138, doi: 10.5505/pajes.2020.76399.

[16] Kooi, T. *et al.* 2017. Large scale deep learning for computer aided detection of mammographic lesions. Med. Image Anal., 35, 303–312, doi: 10.1016/j.media.2016.07.007.

[17] Souza, J. C. Bandeira Diniz, J. O. Ferreira, J. L. França da Silva, G. L. Corrêa Silva, A. de Paiva, A. C. 2019. An automatic method for lung segmentation and reconstruction in chest X-ray using deep neural networks. Comput. Methods Programs Biomed., 177, 285–296, 2019, doi: 10.1016/j.cmpb.2019.06.005.

[18] Gaál, G. Maga, B. Lukács, A. 2020. Attention U-net based adversarial architectures for chest X-ray lung segmentation. CEUR Workshop Proc., 2692, 1–7.

[19] Başaran, E. 2022. Classification of white blood cells with SVM by selecting SqueezeNet and LIME properties by mRMR method. Signal, Image Video Process., doi: 10.1007/s11760-022-02141-2.

[20] Talo, M. Yildirim, O. Baloglu, U. B. Aydin, G. Acharya, U. R. 2019. Convolutional neural networks for multi-class brain disease detection using MRI images. Comput. Med. Imaging Graph., 78, 101673, doi: 10.1016/j.compmedimag.2019.101673.

[21] Yıldırım, Ö. Pławiak, P. Tan, R. S. Acharya, U. R. 2018. Arrhythmia detection using deep convolutional neural network with long duration ECG signals. Comput. Biol. Med., 102(September), 411–420, doi: 10.1016/j.compbiomed.2018.09.009.

[22] Hannun A. Y. *et al.* 2019. Cardiologist-level arrhythmia detection and classification in ambulatory

electrocardiograms using a deep neural network. Nat. Med., 25(1), 65–69, 2019, doi: 10.1038/s41591-018-0268-3.

[23] Acharya, U. R. *et al.*, 2017. A deep convolutional neural network model to classify heartbeats. Comput. Biol. Med., 89(August), 389–396, doi: 10.1016/j.compbiomed.2017.08.022.

[24] Rajpurkar , P. *et al.* 2017. CheXNet: Radiologist-Level Pneumonia Detection on Chest X-Rays with Deep Learning. arxiv, 3–9, http://arxiv.org/abs/1711.05225.

[25] ÇALIŞAN , M. TALU, M. F. 2020. Comparison of Methods for Determining Activity from Physical Movements. J. Polytech., 0900(1), 17–23, doi: 10.2339/politeknik.632070.

[26] Özcan, T. 2020. Yığınlanmış Özdevinimli Kodlayıcılar ile Göğüs Kanserinin Sınıflandırılması ve Klasik Makine Öğrenme Metotları ile Performans Karşılaştırması. Erciyes Univ. J. Institue Sci. Technol., 36(2), 2020, https://dergipark.org.tr/tr/pub/erciyesfen/726739.

[27] Bozdag, Z. Talu,F. M. 2021. Pyramidal nonlocal network for histopathological image of breast lymph node segmentation. Int. J. Comput. Intell. Syst., 14(1), 122–131, doi: 10.2991/ijcis.d.201030.001.

[28] Sun , Y. *et al.* 2021. Multi-Site Infant Brain Segmentation Algorithms: The iSeg-2019 Challenge. IEEE Trans. Med. Imaging, 40(5), 1363–1376, 2021, doi: 10.1109/TMI.2021.3055428.

[29] Subramanian, N. Elharrouss, O. Al-Maadeed, S. Chowdhury, M. 2022. A review of deep learning-based detection methods for COVID-19. Comput. Biol. Med., 143, 105233,doi: 10.1016/j.compbiomed.2022.105233.

[30] Valizadeh , M. Wolff, S. J. 2022. Convolutional Neural Network applications in additive manufacturing : A review. Adv. Ind. Manuf. Eng., 4, 100072, doi: 10.1016/j.aime.2022.100072.

[31] Lecun, Y. Bengio, Y. Hinton, G. 2015. Deep learning. Nature, 521(7553), 436–444, doi: 10.1038/nature14539.

[32] Ulyanov, D. Vedaldi, A. Lempitsky, V. 2016. Instance Normalization: The Missing Ingredient for Fast Stylization. arxiv, http://arxiv.org/abs/1607.08022.

[33] Cirillo, M. D. Abramian, D. Eklund, A. 2020. Vox2Vox: 3D-GAN for Brain Tumour Segmentation. arXiv, 1–10.

[34] Gao, B. Pavel, L. 2017. On the Properties of the Softmax Function with Application in Game Theory and Reinforcement Learning,. arxiv, 1–10, http://arxiv.org/abs/1704.00805.

[35] Han, S. Shao , H. Huo, Z. Yang,X. and Cheng, J, 2022. End-to-end chiller fault diagnosis using fused attention mechanism and dynamic cross-entropy under imbalanced datasets. Build. Environ., 212, 108821, doi: 10.1016/j.buildenv.2022.108821.

[36] Jain, S. Shukla,S. and Wadhvani, R, 2018. Dynamic selection of normalization techniques using data complexity measures. Expert Syst. Appl., 106(252–262), doi: 10.1016/j.eswa.2018.04.008.

[37] Çiçek, Ö. Abdulkadir, A. Lienkamp, S. S. Brox, T. Ronneberger, O. 2016. 3D U-Net: Learning Dense Volumetric Segmentation from Sparse Annotation. Medical Image Computing and Computer-Assisted Intervention, 424–432.